Comparative Analysis of Posture Controllers for Tracking Control of a Four-Wheeled Skid-Steered Mobile Robot in Case of Non-Zero Initial Position and Course Errors

Maciej Trojnacki, Przemysław Dąbek

Abstract— The paper is concerned with the problem of trajectory tracking control of a four-wheeled skid-steered mobile robot in case of non-zero initial position and course (posture) errors. Object of the research, its kinematics and dynamics were described. Structure of robot motion control system containing posture controller and drive controller is shown. Six solutions of the posture controller which allow realization of tracking control as well as a methodology of controller tuning are presented. Effectiveness of particular solutions of posture controller is benchmarked in the simulation studies. Evaluation of the analyzed solutions is carried out using the introduced quality indexes.

Index Terms— wheeled mobile robot, dynamics model, drive model, wheel slips, tracking control, posture controller, drive controller, controller tuning, comparative analysis, simulation research.

1 Introduction

Tracking control, which is the kind of control where chosen point of a robot has to move on certain desired motion trajectory, belongs to important problems of control theory and robotics. From the point of view of synthesis of control systems, wheeled mobile robots can be divided in two categories: robots for which in typical operating conditions there is almost no wheel sliding on the ground during motion, and robots with all wheels non-steered for which wheel sliding is an inherent feature of motion (skid-steered robots). Examples of the robots from the first category are Pioneer 2DX and Azimut [8], whereas from the second category, majority of the robots made by Industrial Research Institute for Automation and Measurements PIAP [22].

In case of the skid-steered robots it is not possible to guarantee satisfactory accuracy of motion realization using the wheel velocity controller only, because of the occurring wheel slips. Better accuracy can be achieved using the robot mobile platform velocity controller, and even better, using the robot position and course, or posture, controller.

The task of this kind of controller is determination of control signals, i.e., robot motion velocities so as to minimize position and course errors, that is the robot posture errors.

As far as mobile robot posture controllers are concerned, the following solutions are usually used: back-stepping method [5], [6], sliding mode method [9] or switching control approach [15], robust control [11], adaptive control [14] using artificial neural networks [1] or fuzzy logic [7] and various hybrid strategies.

In articles [18], [19] the problem of trajectory tracking control of a four-wheeled mobile robot with non-steered wheels using various existing solutions of posture controller was considered in case of zero initial posture error. In those works some modifications of the solutions of posture controller aimed at removing certain limitations were proposed. Additionally, for each solution methodology of controller tuning was described for certain assumed robot boundary velocities and maximum posture errors. A comparative analysis of performance of different controller solutions was conducted by means of simulation studies.

The present article is continuation of the mentioned works aimed at investigations of the analogous solutions of the posture controller, but this time in case of non-zero initial position and course error of the robot. Examination of this case is important from the practical point of view, because it is likely that actual initial posture of the robot will be different than desired posture.

2 Four-Wheeled Skid-Steered Mobile Robot

The object of the research is a small four-wheeled mobile robot with all wheels non-steered called PIAP GRANITE. The robot has all wheels driven independently by DC servomotors with gear units and encoders. The current design of the robot is shown in Fig. 1a, and its kinematic structure is presented in Fig. 1b.

It is possible to distinguish the following main components of the robot: 0 – body with frame for installation of the research equipment, 1-4 – wheels with toothed belt pulleys, 5-6 – toothed belts. The drive transmission in each drive unit can be decoupled and also toothed belts can be removed which permits obtaining various configurations of the robot drive system. In this paper, the configuration of the robot with independent driving of all 4 wheels is analysed.

- *Maciej Trojnacki is with Industrial Research Institute for Automation and Measurements PIAP, Al. Jerozolimskie 202, 02-486 Warsaw, Poland mtrojnacki@piap.pl*
- *Przemysław Dąbek is with Industrial Research Institute for Automation and Measurements PIAP, Al. Jerozolimskie 202, 02-486 Warsaw, Poland pdabek@piap.pl*

a) b)

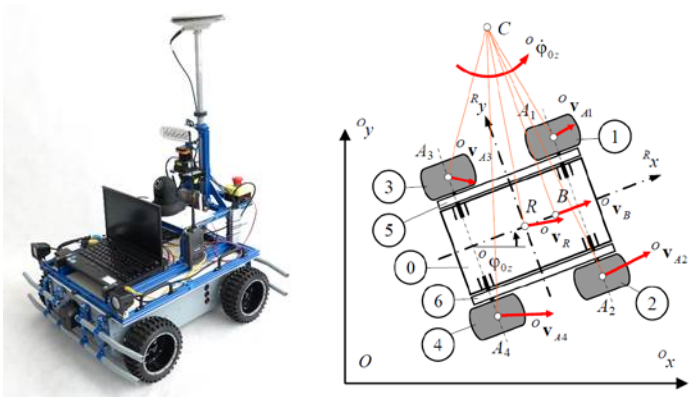

Fig. 1. Four-wheeled skid-steered mobile robot PIAP GRANITE: a – current design, b – kinematic structure

The following symbols for the i^{th} wheel were introduced in the robot model: A_i – geometrical centre, $r_i = r$ – radius, θ_i – angle of wheel spin ($i = 1, ..., 4$).

For robot localization and determination of its motion parameters the inertial measurement units [17], GNSS equipment [12] as well as a 2D laser scanner and maps of environment [3] are used.

3 Modelling of the Robot

3.1 Robot kinematics

It is assumed that robot motion is realized in *Oxy* plane of the fixed coordinate system {*O*}. The moving coordinate system {*R*} is considered to be rigidly connected to the robot. Position and orientation of the mobile platform are described by the vector of generalized coordinates:

$$ {}^{O}\mathbf{q} = [{}^{O}x_R,\ {}^{O}y_R,\ {}^{O}\varphi_{0z}]^T, \tag{1} $$

where: ${}^{O}x_R$, ${}^{O}y_R$ are coordinates of the point *R* of the mobile platform, and ${}^{O}\varphi_{0z} = \psi$ denotes angle of spin of mobile platform about *z* axis with respect to fixed coordinate system {*O*}, also named the course angle.

In turn, vectors of generalized velocities respectively in {*O*} and {*R*} coordinate systems can be written as:

$$ {}^{O}\dot{\mathbf{q}} = \left[{}^{O}\dot{x}_R,\ {}^{O}\dot{y}_R,\ {}^{O}\dot{\varphi}_{0z}\right]^T, \quad {}^{R}\dot{\mathbf{q}} = \left[{}^{R}v_{Rx},\ {}^{R}v_{Ry},\ {}^{R}\dot{\varphi}_{0z}\right]^T, \tag{2} $$

where: ${}^{O}v_{Rx} = {}^{O}\dot{x}_R$, ${}^{O}v_{Ry} = {}^{O}\dot{y}_R$, ${}^{O}\omega_{0z} = {}^{O}\dot{\varphi}_{0z}$.

If one makes assumption that ${}^{R}v_{Ry} \approx 0$ and motion is realized in *Oxy* plane then vector of generalized velocities ${}^{O}\dot{\mathbf{q}}$ can be defined on the basis of kinematic equations of motion in the form:

$$ {}^{O}\dot{\mathbf{q}} = \begin{bmatrix} {}^{O}\dot{x}_R \\ {}^{O}\dot{y}_R \\ {}^{O}\dot{\varphi}_{0z} \end{bmatrix} = \begin{bmatrix} \cos({}^{O}\varphi_{0z}) & 0 \\ \sin({}^{O}\varphi_{0z}) & 0 \\ 0 & 1 \end{bmatrix} \begin{bmatrix} {}^{R}v_{Rx} \\ {}^{R}\dot{\varphi}_{0z} \end{bmatrix}, \tag{3} $$

where vector ${}^{R}\mathbf{v} = [{}^{R}v_{Rx}, {}^{R}\dot{\varphi}_{0z}]^T$ contains respectively component of velocity of the point *R* of the robot on the *x* direction of {*R*} coordinate system and yaw rate of the mobile platform.

In case of plane motion of the mobile platform, velocity of the point *R* depends on angular velocity ${}^{R}\dot{\varphi}_{0z}$ and radius of curvature R_z of the path according to the formula:

$$ {}^{R}v_{Rx} = {}^{R}\dot{\varphi}_{0z}\, R_z, \tag{4} $$

where ${}^{R}v_{Rx}$ is the velocity of the point *R* motion expressed in the coordinates of the reference frame {*R*} associated with the robot.

3.2 Dynamics model of the robot

In this work, dynamics model of the PIAP GRANITE robot which includes wheel slips, developed in [16], will be used. This model will be employed in simulation-based research of posture controller.

Normal components of reactions of the ground can be determined from relationship:

$$ {}^{R}F_{Aiz} = m_R\left((\mp {}^{R}a_{CMx}/(2L) \mp {}^{R}a_{CMy}/(2W))(r + {}^{R}z_{CM}) + g(1/4 \pm {}^{R}x_{CM}/(2L))\right), \tag{5} $$

where actual plus and minus signs depend on the considered wheel.

On the assumption that the robot wheels neither move nor rotate backwards, the current value of longitudinal slip ratio is determined from the formula:

$$ \lambda_i = \begin{cases} 0 \quad \text{for} \quad {}^{R}v_{Aix} = 0 \ \text{and} \ v_{oi} = 0, \\ (v_{oi} - {}^{R}v_{Aix}) / \max({}^{R}v_{Aix}, v_{oi}) \quad \text{for other} \quad {}^{R}v_{Aix} \ \text{and} \ v_{oi}, \end{cases} \tag{6} $$

where $v_{oi} = \dot{\theta}_i\, r_i$ and ${}^{R}v_{Aix}$ are respectively velocity at the wheel circumference and longitudinal component of velocity of wheel geometric center.

Current value of the lateral slip angle is determined from the formula:

$$ \alpha_i = \begin{cases} 0 & \text{for} \quad {}^{R}v_{Aiy} = 0, \\ \operatorname{atan2}({}^{R}v_{Aiy}, |{}^{R}v_{Aix}|) & \text{for} \quad |{}^{R}v_{Aiy}| > 0, \end{cases} \tag{7} $$

where ${}^{R}v_{Aix}$ and ${}^{R}v_{Aiy}$ are respectively longitudinal and lateral velocity of the geometric center of the *i*-th wheel.

In turn, the current value of the tire adhesion coefficient on longitudinal direction for wheel is calculated using Kiencke tire model [13] modified in [16] to the form:

$$ \mu_{ix} = \begin{cases} \dfrac{2\mu_p \lambda_p \lambda_i}{\lambda_p^2 + \lambda_i^2} & \text{for} \quad |\lambda_i| \le \lambda_p, \\ a_{\lambda x}\lambda_i + b_{\lambda x}\operatorname{sgn}(\lambda_i) & \text{for} \quad |\lambda_i| > \lambda_p, \end{cases} \tag{8} $$

where λ_p denotes the value of longitudinal slip corresponding to the value of maximum tire adhesion coefficient μ_p and sgn() is a signum function.

Knowing the lateral slip angle it is possible to calculate current value of the adhesion coefficient on lateral direction for wheel using the following approximate relationship (as compared to H.B. Pacejka model [10], [21]):

$$\mu_{iy} = -\mu_{ymax} \sin(\alpha_i), \tag{9}$$

where μ_{ymax} denotes maximum value of adhesion coefficient on lateral direction.

Longitudinal and lateral components of ground reaction force for the wheel depend on current values of the adhesion coefficient on that directions, according to relationships:

$$^{R}F_{Aix} = \mu_{ix}\, ^{R}F_{Aiz}, \quad ^{R}F_{Aiy} = \mu_{iy}\, ^{R}F_{Aiz}. \tag{10}$$

Then, it is possible to calculate values of accelerations on longitudinal and lateral direction using equations:

$$^{R}a_{CMx} = \sum_{i=1}^{4} {}^{R}F_{Aix}/m_R, \quad ^{R}a_{CMy} = \sum_{i=1}^{4} {}^{R}F_{Aiy}/m_R. \tag{11}$$

For the robot mobile platform, it is also possible to determine angular acceleration $^{R}\ddot{\varphi}_{0z}$ resulting from the dynamic equation of its rotation about *Rz* axis, that is:

$$\begin{aligned} ^{R}\ddot{\varphi}_{0z} = \big(&-(^{R}F_{A1x}+{}^{R}F_{A3x})(W/2-{}^{R}y_{CM})+(^{R}F_{A2x}+{}^{R}F_{A4x})(W/2+{}^{R}y_{CM})+ \\ &+(^{R}F_{A1y}+{}^{R}F_{A2y})(L/2-{}^{R}x_{CM})-(^{R}F_{A3y}+{}^{R}F_{A4y})(L/2+{}^{R}x_{CM})\big)/I_{Rz}, \end{aligned} \tag{12}$$

where I_{Rz} is mass moment of inertia of the robot about the *Rz* axis.

Then, one can calculate by integration the value of angular velocity of the robot mobile platform about this axis, that is $^{R}\dot{\varphi}_{0z}$, as well as values of velocities $^{R}v_{Rx}$ and $^{R}v_{Ry}$ and finally values of velocities of characteristic points A_i.

It is also possible to determine angular parameters of wheel spin, i.e., $\dot{\theta}_i$ and $\ddot{\theta}_i$ for driving torques τ_i acting on the driven wheels based on the equation:

$$\ddot{\theta}_i = \big(\tau_i - {}^{R}F_{Aix}r - {}^{R}F_{Aiz}r\, f_r \operatorname{sgn}(\dot{\theta}_i)\big)/I_{Wy}. \tag{13}$$

where: I_{Wy} – mass moment of inertia of the wheel about its spin axis, f_r – coefficient of rolling resistance.

3.3 Drive units model

It is assumed that: each of the robot drive units consists of identical DC motor, encoder, and transmission system, robot drive units are not self-locking, mass moments of inertia of the rotating elements of DC motor, encoder and gear unit are small in comparison to mass moments of inertia of the driven parts of the robot (wheels), that is why they are neglected.

The model of the i^{th} drive unit is described by dependences:

$$\frac{\mathrm{d}i_i}{\mathrm{d}t} = \big(u_i - k_e n_d \dot{\theta}_i - R_d i_i\big)/L_d, \quad \tau_i = \eta_d n_d k_m i_i, \tag{14}$$

where: u_i – motor voltage input, i_i – rotor current, L_d, R_d – respectively inductance and resistance of the rotor winding, k_e – electromotive force constant, k_m – motor torque coefficient, n_d – gear ratio of the transmission system, η_d – efficiency factor of the transmission system.

4 Posture Controller

4.1 Desired motion and errors

In the control of posture of the robot, one assumes that motion of the robot is realized based on the desired vector of its posture (i.e. position and course), which has the form:

$$^{O}\mathbf{q}_d = \big[{}^{O}x_{Rd},\ {}^{O}y_{Rd},\ {}^{O}\varphi_{0zd}\big]^T, \tag{15}$$

where: $^{O}x_{Rd}$, $^{O}y_{Rd}$ – desired coordinates of characteristic point *R* of the robot in the {*O*} coordinate system in (m), $^{O}\varphi_{0zd} = \psi_d$ – desired course of the mobile platform with respect to *z*-axis of {*O*} coordinate system in (rad).

Desired trajectory of robot motion can be also represented in the form of vector of desired generalized velocities $^{O}\mathbf{v}_d = [{}^{O}v_{Rd},\ {}^{O}\omega_{0zd}]^T$, which corresponds to the vector of desired generalized coordinates $^{O}\mathbf{q}_d$, where: $^{O}v_{Rd}$, $^{O}\omega_{0d} = {}^{O}\dot{\varphi}_{0zd}$ – respectively desired linear velocity of the characteristic point *R* of the robot in (m/s) and desired angular velocity of its mobile platform in (rad/s), in the fixed coordinate system {*O*}.

Moreover, it is assumed that $^{O}v_{Rd} = {}^{R}v_{Rd}$ and $^{O}\dot{\varphi}_{0zd} = {}^{R}\dot{\varphi}_{0zd}$, that is, as a result of the fact that the robot moves on a horizontal plane and values of the linear velocity and angular yaw velocity are independent of the chosen reference frame.

The errors of robot position and course in the moving {*R*} and in the fixed {*O*} coordinate systems can be determined from the relationships:

$$\begin{aligned} ^{R}\mathbf{q}_e &= \begin{bmatrix} {}^{R}e_F \\ {}^{R}e_L \\ {}^{R}e_O \end{bmatrix} = \begin{bmatrix} \cos({}^{O}\varphi_{0z}) & \sin({}^{O}\varphi_{0z}) & 0 \\ -\sin({}^{O}\varphi_{0z}) & \cos({}^{O}\varphi_{0z}) & 0 \\ 0 & 0 & 1 \end{bmatrix} {}^{O}\mathbf{q}_e, \\ ^{O}\mathbf{q}_e &= \begin{bmatrix} {}^{O}e_{Rx} \\ {}^{O}e_{Ry} \\ {}^{O}e_{\psi} \end{bmatrix} = \begin{bmatrix} {}^{O}x_{Rd} - {}^{O}x_R \\ {}^{O}y_{Rd} - {}^{O}y_R \\ {}^{O}\varphi_{0zd} - {}^{O}\varphi_{0z} \end{bmatrix}, \end{aligned} \tag{16}$$

where $^{R}e_F$, $^{R}e_L$, $^{R}e_O$ are respectively longitudinal position error in (m), lateral position error in (m), and course error in (rad).

In Fig. 2, robot desired and actual postures as well as posture errors are illustrated.

It is assumed that $^{O}v_R = {}^{R}v_R \approx {}^{R}v_{Rx}$, that is motion in the ^{R}y axis direction with velocity $^{R}v_{Ry}$ can occur, but $|{}^{R}v_{Ry}| \ll |{}^{R}v_{Rx}|$.

It should be noted that because of kinematic constraints: $^{O}\dot{\varphi}_{0z} = \dot{\varphi}_{0zmin} = 0$ for $|{}^{O}v_R| = v_{Rmax}$ and $^{O}v_R = v_{Rmin} = 0$ for $|{}^{O}\dot{\varphi}_{0z}| = \dot{\varphi}_{0zmax}$.

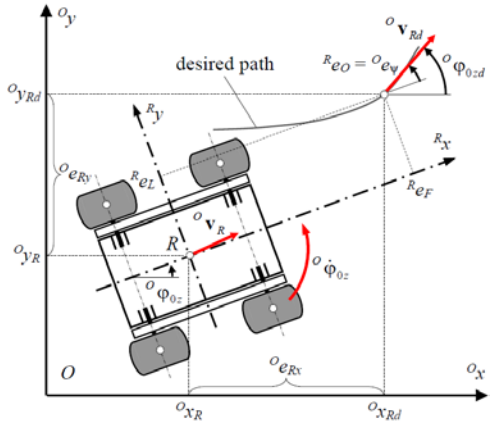

Fig. 2. Desired and actual postures and errors of posture of a robot

4.2 Structure of analyzed control system

A schematic diagram of the robot tracking control system containing posture controller is shown in Fig. 3. Note that the posture controller apart from the position and course errors ${}^{R}\mathbf{q}_e$ requires also desired generalized velocities ${}^{O}\mathbf{v}_d$ to be known.

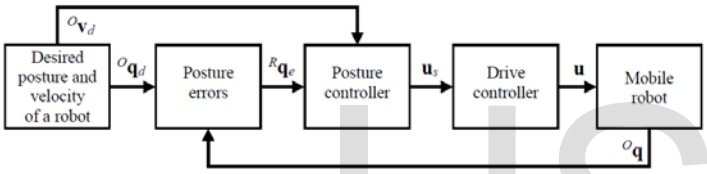

Fig. 3. Schematic diagram of control system of robot motion

The control signal vector $\mathbf{u}_s = [{}^{R}v_s, {}^{R}\omega_s]^T$ contains generalized velocities of motion of the mobile platform expressed in the robot coordinate system $\{R\}$, that is, linear velocity of characteristic point R in (m/s) and angular velocity of the mobile platform in (rad/s), which have appropriate values so as to minimize the posture errors. In a sense, it is a modification of the desired generalized velocities vector as a result of the occurrence of posture errors.

4.3 Velocity limits for posture controllers

It is assumed that each posture controller should generate maximum velocities respectively equal to $v_{smax} = \dot{\theta}_{max} r / 2$, and $\omega_{smax} = v_{smax} / W$. The assumed velocity v_{smax} corresponds to half of the maximum velocity of longitudinal motion of the robot equal to $v_{Rmax} = 1.525$ m/s in the analyzed case.

As far as $\dot{\varphi}_{0zmax}$ and ω_{smax} are concerned, if the wheel slips were absent during robot turning, it would be possible to assume $\dot{\varphi}_{0zmax} = 2\, v_{Rmax} / W$ and $\omega_{smax} = 2\, v_{smax} / W$. Maximum angular velocity of turning of the robot is chosen on assumption that longitudinal slips of wheels can be as high as 50%, which follows from the fact that in the analyzed case robot wheels are not steered. The chosen maximum velocities v_{smax} and ω_{smax} to be generated by the controller guarantee possibility of realization of those velocities for their arbitrary combination, on assumption that for actual robot velocity of turning holds $\dot{\varphi}_{0zmax} = \dot{\theta}_{max} r / W$ (rad/s).

4.4 Selected solutions of posture controllers

In the present work the selected solutions of posture controller are considered with their modifications proposed in [18]. The modifications were aimed at solving problems occurring in case of non-zero initial and final errors and in case of problems associated with large course error.

Finite values of errors of longitudinal position, lateral position and course are assumed. Also it is assumed that the course error is in the range of $\langle -\pi, \pi \rangle$ (rad).

The control signal of posture controller can be determined based on the following solutions modified as mentioned before.

1. Solution based on work of Y. Kanayama et al. [6]:

$$\mathbf{u}_{s1} = \begin{bmatrix} {}^{R}v_{s1} \\ {}^{R}\omega_{s1} \end{bmatrix} = \begin{bmatrix} k_F\, {}^{R}e_F\, |\mathrm{sgn}({}^{O}v_{Rd})| + {}^{O}v_{Rd}\, f_v({}^{R}e_O) \\ {}^{O}\dot{\varphi}_{0zd} + k_L\, {}^{O}v_{Rd}\, {}^{R}e_L + k_O\, {}^{O}v_{Rd}\, f_\omega({}^{R}e_O) \end{bmatrix}, \tag{17}$$

where: k_F (s^{-1}), k_L (m^{-2}), k_O (m^{-1}) – chosen positive parameters.

2. Solution based on work of M. Cao [2]:

$$\mathbf{u}_{s2} = \begin{bmatrix} {}^{R}v_{s2} \\ {}^{R}\omega_{s2} \end{bmatrix} = \begin{bmatrix} k_F\, {}^{R}e_F\, |\mathrm{sgn}({}^{O}v_{Rd})| + {}^{O}v_{Rd}\, f_v({}^{R}e_O) \\ {}^{O}\dot{\varphi}_{0zd} + k_\psi\, |{}^{R}e_O|^{a} \tanh(k_\omega\, {}^{R}e_O)\, |\mathrm{sgn}({}^{O}v_{Rd})| \end{bmatrix}, \tag{18}$$

where k_F (s^{-1}), $k_\psi > 0$ (s^{-1}), $0 < a < 1$ (–) – chosen positive parameters.

3. Solution based on work of J.H. Lee et al. [9]:

$$\mathbf{u}_{s3} = \begin{bmatrix} {}^{R}v_{s3} \\ {}^{R}\omega_{s3} \end{bmatrix} = \begin{bmatrix} k_F\, {}^{R}e_L\, {}^{O}\dot{\varphi}_{0z}\, |\mathrm{sgn}({}^{O}v_{Rd})| + {}^{O}v_{Rd}\, f_v({}^{R}e_O) + \\ + k_S\, |\mathrm{sgn}({}^{O}v_{Rd})|\tanh(k_v s_v) \\ {}^{O}\dot{\varphi}_{0zd} + k_L \dfrac{\partial\alpha}{\partial\, {}^{O}v_{Rd}}\, {}^{O}\dot{v}_{Rd} + k_O \dfrac{\partial\alpha}{\partial\, {}^{R}e_L} \left({}^{O}v_{Rd}\, f_\omega({}^{R}e_O) \right) + \\ + k_\psi\, |\mathrm{sgn}({}^{O}v_{Rd})|\tanh(k_\omega s_\omega) \end{bmatrix}. \tag{19}$$

where: k_F (–), k_L (m^{-2}), k_O (m^{-2}), k_S (s^{-1}), k_ψ (s^{-1}) are chosen positive parameters, sat() is a saturation function, $s_v = {}^{R}e_F$, $s_\omega = {}^{R}e_O + \mathrm{atan}({}^{O}v_{Rd}\, {}^{R}e_L)$ and

$$\frac{\partial\alpha}{\partial\, {}^{O}v_{Rd}} = \frac{{}^{R}e_L}{1 + ({}^{O}v_{Rd}\, {}^{R}e_L)^2}, \frac{\partial\alpha}{\partial\, {}^{R}e_L} = \frac{{}^{O}v_{Rd}}{1 + ({}^{O}v_{Rd}\, {}^{R}e_L)^2}. \tag{20}$$

4. Solution based on work of K. Wang et. al. [20], whose original form was proposed by Z.P. Jiang and H. Nijmeijer [5]:

$$\mathbf{u}_{s4} = \begin{bmatrix} {}^{R}v_{s4} \\ {}^{R}\omega_{s4} \end{bmatrix} = \begin{bmatrix} k_F\, {}^{R}e_F\, |\mathrm{sgn}({}^{O}v_{Rd})| + {}^{O}v_{Rd}\, f_v({}^{R}e_O) \\ {}^{O}\dot{\varphi}_{0zd} + k_\psi\, {}^{R}e_O\, |\mathrm{sgn}({}^{O}v_{Rd})| + \\ + k_O\, {}^{O}v_{Rd}\, {}^{R}e_L\, |\, f_\omega({}^{R}e_O)\, |/(|{}^{R}e_O| + {}^{R}e_{Omin}) \end{bmatrix}, \tag{21}$$

where $k_F > 0$ (s^{-1}), $k_\psi > 0$ (s^{-1}), $k_O > 0$ (m^{-2}) are chosen positive parameters.

5. Solution based on work of Z.P. Jiang et al. [4]:

$$\mathbf{u}_{s5} = \begin{bmatrix} {}^R v_{s5} \\ {}^R \omega_{s5} \end{bmatrix} = \begin{bmatrix} k_S \tanh(k_v {}^R e_F) |\operatorname{sgn}({}^O v_{Rd})| + {}^O v_{Rd} f_v({}^R e_O) \\ {}^O \dot{\varphi}_{0zd} + k_\psi \tanh(k_\omega {}^R e_O) |\operatorname{sgn}({}^O v_{Rd})| + \\ + k_O {}^O v_{Rd} {}^R e_L | f_\omega({}^R e_O)| / \left((|{}^R e_O| + {}^R e_{Omin})(1 + {}^R e_F^2 + {}^R e_L^2) \right) \end{bmatrix}. \quad (22)$$

where k_S (m/s), k_ψ (s^{-1}), k_O (–), k_v (m^{-1}) and k_ω (–) – chosen positive parameters.

6. Solution based on work of J.M. Toibero et al. [15]:

$$\mathbf{u}_{s6} = \begin{bmatrix} {}^R v_{s6} \\ {}^R \omega_{s6} \end{bmatrix} = \begin{bmatrix} k_F \dfrac{d}{d + d_{min}} {}^O v_{Rdmax} f_v({}^R e_O) |\operatorname{sgn}({}^O v_{Rd})| \\ \dfrac{{}^O v_{Rd}}{d + d_{min}} f_\omega({}^R e_O) + k_\psi \tanh(k_\omega {}^R e_O) |\operatorname{sgn}({}^O v_{Rd})| \end{bmatrix}, \quad (23)$$

where k_F (–), k_ψ (s^{-1}) – chosen positive parameters, d_{min} – assumed position inaccuracy of the robot.

In this case position and course errors are defined in form of the vector:

$${}^R \mathbf{q}_e = \begin{bmatrix} {}^R d \\ {}^R e_O \end{bmatrix} = \begin{bmatrix} \sqrt{({}^R e_F)^2 + ({}^R e_L)^2} \\ {}^R \varphi_{0zd}^O - {}^R \varphi_{0z}^O \end{bmatrix} = \begin{bmatrix} \sqrt{({}^O e_{Rx})^2 + ({}^O e_{Ry})^2} \\ {}^O \varphi_{0zd} - {}^O \varphi_{0z} \end{bmatrix}. \quad (24)$$

For all above solutions it is assumed in the present work that $f_v = \operatorname{sech}(k_b {}^R e_O)$ and $f_\omega = \tanh(k_b {}^R e_O)$.

4.5 Drive controller

Having control signal $\mathbf{u}_s = [{}^R v_s, {}^R \omega_s]^T$ containing generalized velocities in (m/s) and (rad/s) respectively, the control signal for motors of driven wheels in (V) can be determined using the relationship which results from robot kinematics:

$$\mathbf{u} = \begin{bmatrix} u_l \\ u_r \end{bmatrix} = \operatorname{sat}\left(\frac{k_u}{r} \begin{bmatrix} 1 & -W/2 \\ 1 & W/2 \end{bmatrix} \operatorname{sat}(\mathbf{u}_s, \mathbf{u}_{smin}, \mathbf{u}_{smax}), \mathbf{u}_{min}, \mathbf{u}_{max} \right), \quad (25)$$

where u_l and u_r are control signals for respectively left-hand side and right-hand side wheels of the robot, the parameter k_u = 1 Vs, and $\mathbf{u}_s = \{\mathbf{u}_{s1}, \mathbf{u}_{s2}, \mathbf{u}_{s3}, \mathbf{u}_{s4}, \mathbf{u}_{s5}, \mathbf{u}_{s6}\}$ is a control vector from one of the earlier described solutions of the posture controller, $\mathbf{u}_{smax} = [v_{smax}, \omega_{smax}]^T$, $\mathbf{u}_{smin} = [v_{smin}, -\omega_{smax}]^T$, $\mathbf{u}_{max} = [u_{max}, u_{max}]^T$, $\mathbf{u}_{min} = [u_{min}, u_{min}]^T$, the sat() function is saturation function, $u_{min} = 0$ and $v_{smin} = 0$.

4.6 Posture controller tuning methodology

During posture controller tuning it is assumed that for any time instant t, the following conditions are satisfied:

$$|{}^O v_{Rd}| \le v_{smax} \le v_{Rmax} \text{ and } |{}^O \dot{\varphi}_{0zd}| = |{}^O \omega_{0d}| \le \omega_{smax} \le \dot{\varphi}_{0zmax}, \quad (26)$$

$$|{}^O v_R| \le v_{smax} \text{ and } |{}^O \dot{\varphi}_{0z}| = |{}^O \omega_0| \le \omega_{smax}, \quad (27)$$

that is, desired and actual both linear velocities of the point R and angular velocities of the robot body should be smaller than the certain assumed limits, respectively v_{smax} and ω_{smax}.

It is assumed that tanh() function occurring in solutions no. 3, 5 and 6 should saturate for $\pm\pi$ rad argument value. After assuming that maximum absolute values of longitudinal position error and course error are respectively equal to ${}^R e_{Fmax}$ = 1 m and ${}^R e_{Omax} = \pi/2$ rad, the gains k_v and k_ω for the analyzed solutions of controllers should be respectively equal to π and 2. Values of the critical errors ${}^R e_{Fmax}$, ${}^R e_{Omax}$ should be chosen for a given object in such way that the controller does not generate errors larger than critical. Therefore, they should not be too small, to avoid exceeding the limits easily.

During choice of the remaining parameters for posture controller it is assumed that the controller should generate maximum velocities of v_{smax} or ω_{smax} for minimum or critical posture errors respectively equal to ${}^R e_{Fmin} = 0$, ${}^R e_{Lmin} = 0$, ${}^R e_{Omin} = 0$ and ${}^R e_{Fmax}$ = 1 m, ${}^R e_{Lmax}$ = 1 m, ${}^R e_{Omax} = \pi/2$ rad. Moreover, it is assumed that in case of their exceeding, the controller should still generate maximum velocities v_{smax} or ω_{smax} thanks to use of the saturation function. The case when maximum errors are assumed too large leads to situation where controller gains are relatively small, and as a result the controller is less effective, that is larger tracking errors are generated.

5 Simulation Research

The main part of the present work are simulation studies aimed at evaluation of several solutions of the posture controller in case of non-zero initial position and course error, for the controller parameters chosen according to the proposed methodology.

5.1 Desired trajectory and robot parameters

It is assumed that robot motion consists of three phases: accelerating with maximum acceleration a_{Rmax} over the distance of l_r, steady motion with constant velocity v_{Ru} and braking with maximum acceleration (deceleration) a_{Rmax} over the distance of l_h. The desired path of motion contains straight line segment of length L_p, circular arc of radius R_z and the second straight line segment of length 2 L_p. As a result of turning with maximum angular velocity equal to $\omega_{0zu} = v_{Ru}/R_z$, the robot should turn through the angle of φ_{zmax}.

For the simulation, the maximum values of desired linear and angular velocities are assumed respectively equal to v_{Ru} = 0.3 m/s and $\omega_{0zu} = v_{Ru}/R_z$, maximum acceleration during accelerating and braking phases a_{Rmax} = 0.7 m/s², maximum angular acceleration $\varepsilon_{0zmax} = \pi/4$ rad/s² and length L_p = 1 m.

In the simulation the following three cases of robot motion are considered:

1. soft turning to the right with radius R_z = 1 m and angle of rotation φ_{0zmax} = 2/3 π rad, with non-zero initial posture, that is, ${}^{O}\mathbf{q}(0) = {}^{O}\mathbf{q}_0 = [-0.5\text{ m}, 0.2\text{ m}, \pi/6\text{ rad}]^T$,
2. soft turning to the right with radius R_z = 1 m and angle of rotation φ_{0zmax} = 2/3 π rad, with non-zero initial posture, that is, ${}^{O}\mathbf{q}(0) = {}^{O}\mathbf{q}_0 = [-0.5\text{ m}, -0.2\text{ m}, -\pi/6\text{ rad}]^T$, where the difference against case no. 1 is in signs of the ${}^{O}y_0$ and ${}^{O}\varphi_{0z}$ coordinates,
3. rapid turning to the right with radius R_z = 0.5 m and angle of rotation $\varphi_{0zmax} = \pi$ rad, with non-zero initial posture ${}^{O}\mathbf{q}(0) = {}^{O}\mathbf{q}_0 = [-0.5\text{ m}, -0.1\text{ m}, \pi/3\text{ rad}]^T$.

In all above cases, zero initial conditions concerning robot velocities are assumed.

Lengths of acceleration and braking distances, l_r and l_h respectively, are determined for the given velocity profile based on v_{Ru} velocity and maximum acceleration a_{Rmax}.

Next, based on the knowledge of v_{Ru} and ω_{0zu} velocities, a_{Rmax} and ε_{0zmax} accelerations, the L_p length and characteristic time instants are determined.

For the simulation studies the following values of the basic design parameters of the PIAP GRANITE robot are assumed:

- dimensions: L = 0.425 m, W = 0.553 m (where: $L = A_1A_3 = A_2A_4$, $W = A_1A_2 = A_3A_4$, see Fig. 1b), $r_i = r$ = 0.0965 m,
- masses of the components: m_0 = 40 kg, m_i = 1 kg,
- robot mass center coordinates: ${}^{R}x_{CM}$ = –0.04 m, ${}^{R}y_{CM} \approx 0$ m, ${}^{R}z_{CM}$ = 0.14 m,
- mass moments of inertia: I_{Wy} = 0.01 kg m², I_{Rz} = 2.8 kg m²,
- parameters of drive units: L_d = 0.0823 mH, R_d = 0.317 Ω, k_e = 0.0301 Vs/rad, k_m = 0.0302 Nm/A, n_d = 53, η_d = 0.8, $\dot{\theta}_{max}$ = 15.807 rad/s, $\dot{\theta}_{min}$ = 0, u_{max} = 32 V, u_{min} = 0.

Moreover, the following environment and tire-ground contact parameters are assumed: g = 9.81 m/s², μ_p = 0.85, μ_s = 0.75, f_r = 0.03, λ_p = 16.5%.

The desired motion paths and time histories of desired velocities and accelerations of robot motion are illustrated in Fig. 4.

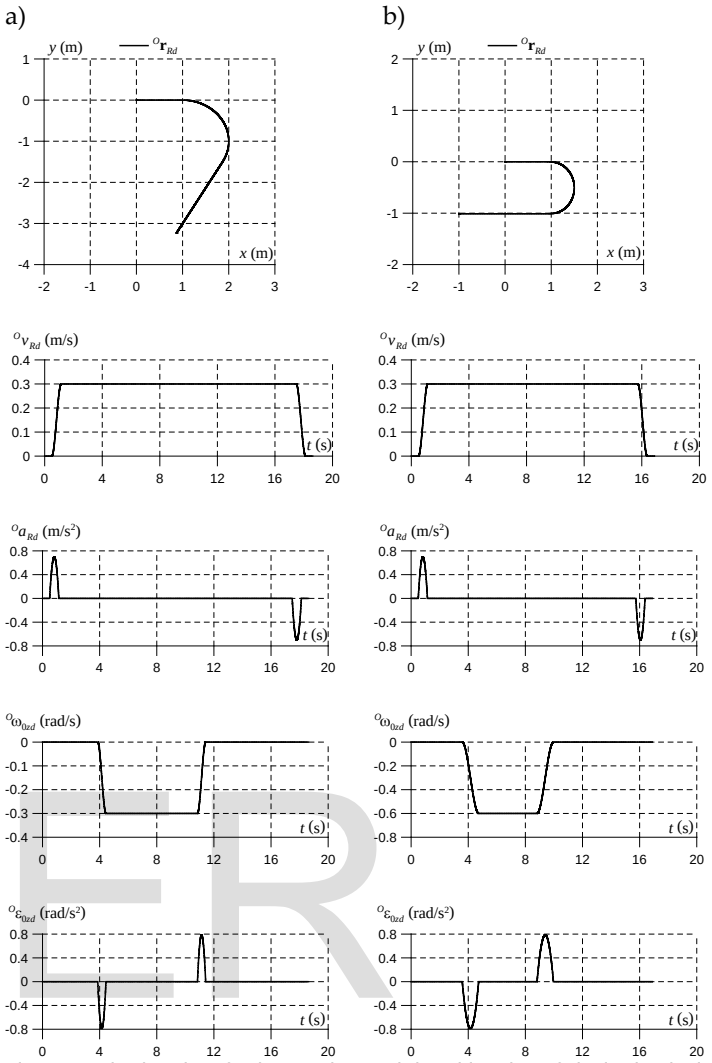

Fig. 4. Desired paths of robot motion and time histories of desired velocities and accelerations: a – soft turning to the right with radius R_z = 1 m and angle of turn φ_{0zmax} = 2/3 π rad, b – rapid turning to the right with radius R_z = 0.5 m and angle of turn φ_{0zmax} = π rad

5.2 Quality indexes

In order to compare in a comprehensive way accuracy of realization of motion by the robot for the analyzed solutions of posture controller, the following quality indexes were introduced during the simulation studies:

- maximum posture errors of the robot:

$${}^{R}e_{Fmax} = \max_{t\in\langle 0,T\rangle}\left(\left|{}^{R}e_F\right|\right),\quad {}^{R}e_{Lmax} = \max_{t\in\langle 0,T\rangle}\left(\left|{}^{R}e_L\right|\right),\quad {}^{R}e_{Omax} = \max_{t\in\langle 0,T\rangle}\left(\left|{}^{R}e_O\right|\right), \tag{28}$$

- square root of integral of the squared error for each robot posture error:

$$E_F = \sqrt{\frac{1}{T}\int_0^T \left({}^{R}e_F\right)^2 \mathrm{d}t},\quad E_L = \sqrt{\frac{1}{T}\int_0^T \left({}^{R}e_L\right)^2 \mathrm{d}t},\quad E_O = \sqrt{\frac{1}{T}\int_0^T \left({}^{R}e_O\right)^2 \mathrm{d}t}, \tag{29}$$

- integral of absolute error multiplied by time for each robot posture error:

$$Q_F = \frac{2}{T^2}\int_0^T (|{}^{R}e_F|\,t)\,\mathrm{d}t,\quad Q_L = \frac{2}{T^2}\int_0^T (|{}^{R}e_L|\,t)\,\mathrm{d}t,\quad Q_O = \frac{2}{T^2}\int_0^T (|{}^{R}e_O|\,t)\,\mathrm{d}t, \tag{30}$$

where T is the analyzed time period of robot motion.

All above quality indexes have units analogous to the posture errors. The first quality index enables finding the maximum posture errors. In case of the second index, average errors in the assumed time interval are obtained. The third quality index is designed so as to determine the average errors as well, but this time in the averaging process the time plays a key role, that is the errors occurring closer to the final phase of motion are more important than initial errors, which allows for assessment of how the analyzed controller solution deals with reduction of errors with time.

5.3 Values of controller parameters

For simulation studies, maximum (boundary) values of controller parameters calculated according to the methodology discussed earlier are adopted. Values of those parameters are summarized in Table 1 for the first desired motion trajectory and in Table 2 for the second trajectory.

TABLE 1
ASSUMED VALUES OF POSTURE CONTROLLER PARAMETERS FOR THE FIRST MOTION TRAJECTORY

Posture controller	k_F	k_L	k_O	k_S	k_ψ
No. 1	0.4627	1.3090	2.2883	–	–
No. 2	0.4627	–	–	–	0.8611
No. 3	0.0218	0.0467	0.3633	0.2163	1.0192
No. 4	0.4627	–	0.1000	–	0.6750
No. 5	–	–	0.4729	0.4627	1.0492
No. 6	2.7221	–	–	–	1.1811

TABLE 2
ASSUMED VALUES OF POSTURE CONTROLLER PARAMETERS FOR THE SECOND MOTION TRAJECTORY

Posture controller	k_F	k_L	k_O	k_S	k_ψ
No. 1	0.4627	0.8040	1.7933	–	–
No. 2	0.4627	–	–	–	0.6217
No. 3	0.0218	0.0934	0.7267	0.2163	0.6592
No. 4	0.4627	–	0.2000	–	0.4720
No. 5	–	–	0.9529	0.4627	0.7192
No. 6	2.7221	–	–	–	1.1811

It can be noticed that in case of the posture controller solution no. 6, for constant ${}^{O}v_{Rdmax}$ value and various ${}^{O}\omega_{0dmax}$ values, the controller parameters do not change for the analyzed desired motion trajectories.

In all simulations $f_v = \mathrm{sech}(k_b\ {}^{R}e_O)$ and $f_\omega = \tanh(k_b\ {}^{R}e_O)$ functions with parameter $k_b = 1$ are adopted. Moreover, for the solutions no. 3, 4 and 5 parameter $\eta = 0.1$ is assumed, for the solution no. 2 parameter $a = 0.5$, and finally in the case of solution no. 6, $d_{min} = 0.1$ m.

5.4 Comparative analysis of posture controllers

For the earlier discussed controller solutions and the adopted robot motion trajectories, simulation studied were carried out. Quality indexes obtained for particular simulations are shown in Tables 3-5.

In the case of the first desired motion trajectory and non-zero initial position and course (and in consequence non-zero posture errors), that is, for ${}^{O}\mathbf{q}(0) = {}^{O}\mathbf{q}_0 = [-0.5\text{ m}, 0.2\text{ m}, \pi/6\text{ rad}]^T$ (Table 3) the solution no. 5 was the best in general, and it yielded the lowest values of the ${}^{R}e_{Fmax}$, ${}^{R}e_{Lmax}$, E_F, E_O, Q_F and Q_O quality indexes and low value of the E_L index.

In turn, the lowest value of the ${}^{R}e_{Lmax}$ index was obtained for solution no. 3 and of E_L and Q_L indexes for the solution no. 1. In general, the worst results were obtained for the solution no. 4. The largest spread of the obtained quality index values is associated with solution no. 6, that is some of the indexes are good and the majority is the worst. For all solutions the maximum course error is equal to the initial error ($\pi/6$ rad), so this error is made smaller by all solutions of the posture controller.

TABLE 3
QUALITY INDEXES OBTAINED FOR PARTICULAR CONTROLLERS IN SIMULATION STUDIES, FOR THE FIRST MOTION TRAJECTORY AND NON-ZERO INITIAL POSTURE ${}^{O}\mathbf{q}_0 = [-0.5\text{ m}, 0.2\text{ m}, \pi/6\text{ rad}]^T$

PC	${}^{R}e_{Fmax}$ (m)	${}^{R}e_{Lmax}$ (m)	${}^{R}e_{Omax}$ (rad)	E_F (m)	E_L (m)	E_O (rad)	Q_F (m)	Q_L (m)	Q_O (rad)
1	0.5634	0.4693	0.5236	0.4596	0.2404	0.2387	0.4457	0.0861	0.1462
2	0.6284	0.5083	0.5236	0.4976	0.2914	0.2517	0.4896	0.1284	0.1662
3	0.5364	0.4232	0.5236	0.4043	0.2454	0.1667	0.3559	0.2143	0.1016
4	0.6454	0.5430	0.5236	0.5168	0.3251	0.2790	0.5144	0.2060	0.1875
5	0.3330	0.4232	0.5236	0.2205	0.2555	0.1447	0.1792	0.1777	0.0467
6	0.7707	0.6047	0.5236	0.2640	0.5201	0.1714	0.2397	0.5635	0.0742

For the second desired motion trajectory and ${}^{O}\mathbf{q}_0 = [-0.5\text{ m}, -0.2\text{ m}, -\pi/6\text{ rad}]^T$ unquestionably best results were obtained for the solution no. 5 of the posture controller, which is clearly visible in Table 4. As far as the ${}^{R}e_L$ error is concerned, good results are for solution no. 3, whereas concerning the ${}^{R}e_F$ error, for solution no. 2. The worst results were obtained again for solution no. 6. However, it was observed that in this case better accuracy of motion realization can be achieved by increasing minimum position error d_{min}. It follows that in this particular situation important is the fact that initial position error $d(0)$ is larger than d_{min}. However, this fact is not important in the next analyzed case.

TABLE 4
QUALITY INDEXES OBTAINED FOR PARTICULAR CONTROLLERS IN SIMULATION STUDIES, FOR THE FIRST MOTION TRAJECTORY AND NON-ZERO INITIAL POSTURE ${}^{O}\mathbf{q}_0 = [-0.5\text{ m}, -0.2\text{ m}, -\pi/6\text{ rad}]^T$

PC	${}^{R}e_{Fmax}$ (m)	${}^{R}e_{Lmax}$ (m)	${}^{R}e_{Omax}$ (rad)	E_F (m)	E_L (m)	E_O (rad)	Q_F (m)	Q_L (m)	Q_O (rad)
1	0.5016	0.4678	0.5851	0.3601	0.3037	0.3545	0.3412	0.2041	0.2487
2	0.4619	0.6059	0.5236	0.2851	0.4008	0.2484	0.2223	0.2606	0.1681
3	0.4979	0.4232	0.5236	0.3122	0.2730	0.1938	0.2430	0.2165	0.1172
4	0.4691	0.6367	0.5236	0.2880	0.4094	0.2849	0.2305	0.2166	0.2032
5	0.3330	0.4232	0.5236	0.1619	0.2674	0.1627	0.1062	0.1775	0.0678
6	1.6210	0.9296	0.5236	0.7111	0.6441	0.1700	0.7921	0.7076	0.0739

For the third desired motion trajectory and zero initial conditions the best results were obtained for the solutions no. 6 and 5 of the posture controller, which is illustrated in Table 5. The worst results were obtained for solutions no. 4 and 1. When it comes to the ${}^{R}e_L$ error, good results are obtained for solution no. 3.

TABLE 5
QUALITY INDEXES OBTAINED FOR PARTICULAR CONTROLLERS IN SIMULATION STUDIES, FOR THE SECOND MOTION TRAJECTORY AND NON-ZERO INITIAL POSTURE ${}^{O}\mathbf{q}_0 = [-0.5\text{ m}, -0.1\text{ m}, \pi/3\text{ rad}]^T$

PC	${}^{R}e_{Fmax}$ (m)	${}^{R}e_{Lmax}$ (m)	${}^{R}e_{Omax}$ (rad)	E_F (m)	E_L (m)	E_O (rad)	Q_F (m)	Q_L (m)	Q_O (rad)
1	0.8053	0.6725	1.0472	0.5254	0.3815	0.6347	0.4942	0.2865	0.4599
2	0.7828	0.6339	1.0472	0.4965	0.3252	0.5673	0.4475	0.1779	0.3897
3	0.7293	0.4510	1.0472	0.4149	0.2820	0.4360	0.2863	0.1766	0.2287
4	0.8532	0.7345	1.0472	0.5530	0.4188	0.6723	0.5235	0.3174	0.5198
5	0.3924	0.4684	1.0472	0.2666	0.2629	0.3762	0.2014	0.1441	0.1453
6	0.3936	0.3830	1.0472	0.2533	0.1839	0.3567	0.1968	0.1091	0.1339

In order to choose the optimal solution of the controller for desired motion trajectories and non-zero initial position and coure errors, a total score for each solution was calculated as total sum of the individual quality indexes for particular controller solution divided by the number of performed simulations (Table 6). According to this measure, the solution no. 5 is optimal. The second best one is the solution no. 3. The third best solutions are both the solution no. 1 and 2, for which similar scores were obtained. The worst alternatives are the solutions no. 6 and 4. In the same table are presented for comparison the results obtained in the work [19] for the case of zero initial posture. It can be noticed easily that in case of non-zero initial posture the solution no. 6 performs much worse than in case of zero initial posture. In the other cases the differences are not so pronounced.

In case of positive value of ${}^{O}x_{R0}$ and, in consequence, the negative value of the initial error ${}^{R}e_{F}$ arises the problem of how the robot should behave in such situation, that is, if it should: move backwards or wait until the desired coordinate ${}^{O}x_{Rd}$ is greater than ${}^{O}x_{R0}$, or turn through 180° and then move forwards, etc. Therefore, additional assumptions for the considered controllers should be introduced, possibly complemented with additional controllers responsible for realization of the preferred robot behavior.

TABLE 6
TOTAL SCORES FOR EACH CONTROLLER SOLUTION CALCULATED BASED ON ALL SIMULATIONS

Posture controller		No. 1	No. 2	No. 3	No. 4	No. 5	No. 6
TOTAL SCORE	zero initial posture [19]	3.39	2.92	1.91	3.61	1.37	1.18
	non-zero initial posture	3.95	3.84	3.27	4.21	2.61	4.32

Motion paths of the characteristic point *R* of the robot for all analyzed solutions and cases of robot motion are shown in Fig. 5. Conclusions from their analysis are similar to those from the analysis of the obtained quality indexes.

At the end, , in Figs. 6-14 are presented time histories of velocities, posture errors and control signals for selected solutions of the posture controller for the considered robot motion cases. The results were selected for presentation according to the rule that for each motion case, two best solutions are presented and the worst one.

In Fig. 6 results of the simulation studies for the first desired motion trajectory, for ${}^{O}\mathbf{q}_0 = [-0.5\text{ m}, 0.2\text{ m}, \pi/6\text{ rad}]^T$ and using 5th solution of posture controller are illustrated.

Because of the initial position error, the robot moves at first with larger velocity (Fig. 6a), and because of the initial course error it executes a turn to the right (Fig. 6b). During motion gradually robot posture errors are reduced, however after the planned turn is finished and the course error ${}^{R}e_{O}$ is eliminated, further reduction of the ${}^{R}e_{L}$ error is inhibited due to the limitation of the adopted control law for the robot angular velocity ${}^{R}\omega_{s}$.

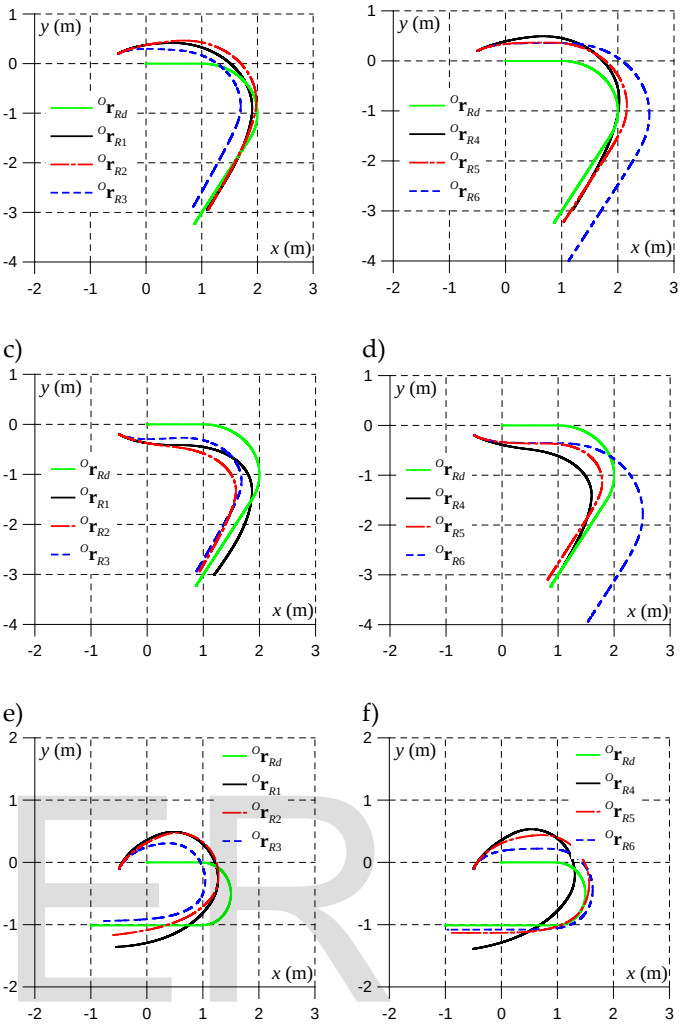

Fig. 5. Motion paths of the point *R* of the robot for particular solutions: a, b – for the first desired motion trajectory and ${}^{O}\mathbf{q}_0 = [-0.5\text{ m}, 0.2\text{ m}, \pi/6\text{ rad}]^T$, c, d – for the first desired motion trajectory and ${}^{O}\mathbf{q}_0 = [-0.5\text{ m}, -0.2\text{ m}, -\pi/6\text{ rad}]^T$, e, f – for the second desired motion trajectory and ${}^{O}\mathbf{q}_0 = [-0.5\text{ m}, -0.1\text{ m}, \pi/3\text{ rad}]^T$

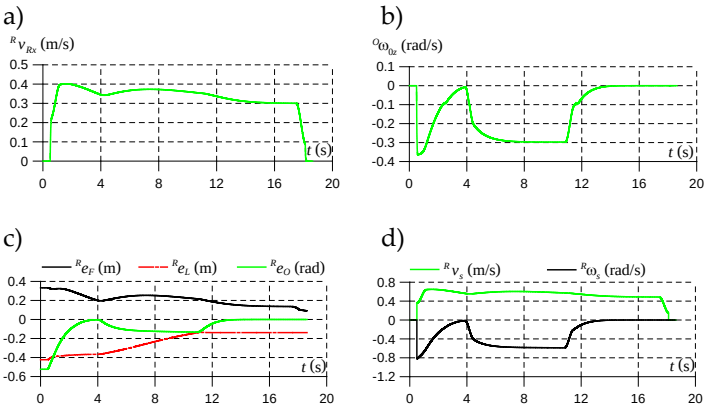

Fig. 6. Time histories of velocities, errors and control signals for the first desired motion trajectory, ${}^{O}\mathbf{q}_0 = [-0.5\text{ m}, 0.2\text{ m}, \pi/6\text{ rad}]^T$ and the posture controller solution no. 5

As shown in Fig. 7, quite good results are also obtained for the posture controller solution no. 3.

In Fig. 8 results of simulation studies for the analyzed motion case for solution no. 6 are shown.

For this solution unquestionably the worst results are obtained considering the ${}^{R}e_{L}$ error, which is not reduced by the controller. After the motion is finished, large negative ${}^{R}e_{F}$ error remains and towards the end of motion the control signal ${}^{R}v_{s}$ attains the value close to maximum, that is ${}^{R}v_{smax}$.

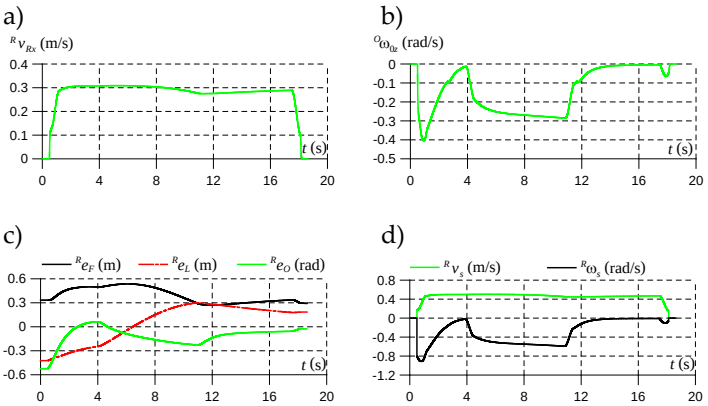

Fig. 7. Time histories of velocities, errors and control signals for the first desired motion trajectory, ${}^{O}\mathbf{q}_{0}$ = [–0.5 m, 0.2 m, π/6 rad]^{T} and the posture controller solution no. 3

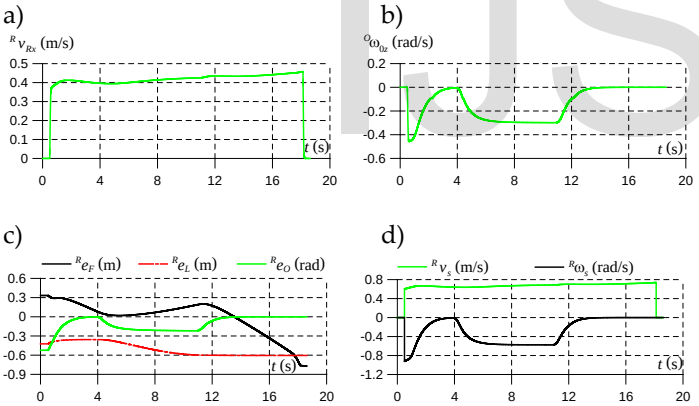

Fig. 8. Time histories of velocities, errors and control signals for the first desired motion trajectory, ${}^{O}\mathbf{q}_{0}$ = [–0.5 m, 0.2 m, π/6 rad]^{T} and the posture controller solution no. 6

In the next three figures are shown results of simulation studies for the same desired trajectory of motion, but for initial posture ${}^{O}\mathbf{q}_{0}$ = [–0.5 m,–0.2 m,–π/6 rad]^{T}. In Fig. 9 results for solution no. 5 of the posture controller are presented. This time during robot motion significant changes in linear velocity can be noticed (Fig. 9a). As previously, the course error ${}^{R}e_{O}$ is reduced to zero, whereas the ${}^{R}e_{F}$ and ${}^{R}e_{L}$ errors are reduced but not completely eliminated. The control signals ${}^{R}v_{s}$ and ${}^{R}\omega_{s}$ do not exceed the assumed boundary values.

In the case of posture controller solution no. 3, changes in linear velocity can be noticed and it can be seen that in certain phases of movement it is smaller in comparison to the desired velocity (Fig. 10a). It can be observed that ${}^{R}e_{F}$ and ${}^{R}e_{L}$ errors are not completely eliminated and have quite large maximum values, while at the end ${}^{R}e_{O}$ error is close to zero (Fig. 10c).

This time, the worst results for the solution no. 6 were obtained (Fig. 11). This controller eliminates mainly the course error ${}^{R}e_{O}$ (Fig. 11c), but poorly deals with the other types of errors.

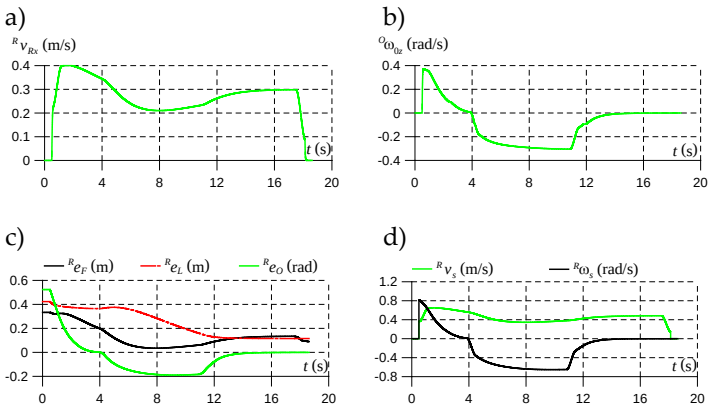

Fig. 9. Time histories of velocities, errors and control signals for the first desired motion trajectory, ${}^{O}\mathbf{q}_{0}$ = [–0.5 m,–0.2 m,–π/6 rad]^{T} and the posture controller solution no. 5

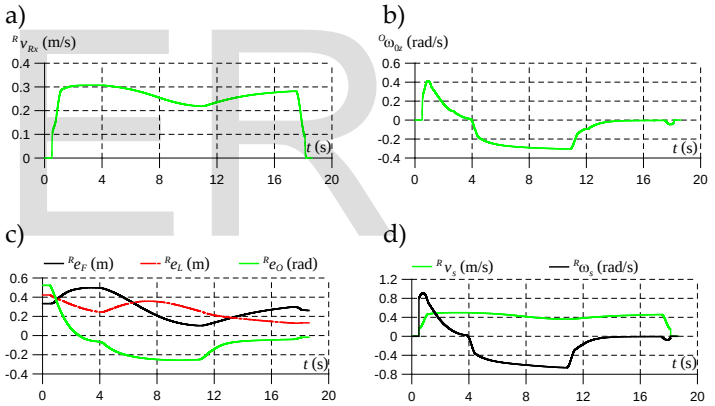

Fig. 10. Time histories of velocities, errors and control signals for the first desired motion trajectory, ${}^{O}\mathbf{q}_{0}$ = [–0.5 m,–0.2 m,–π/6 rad]^{T} and the posture controller solution no. 3

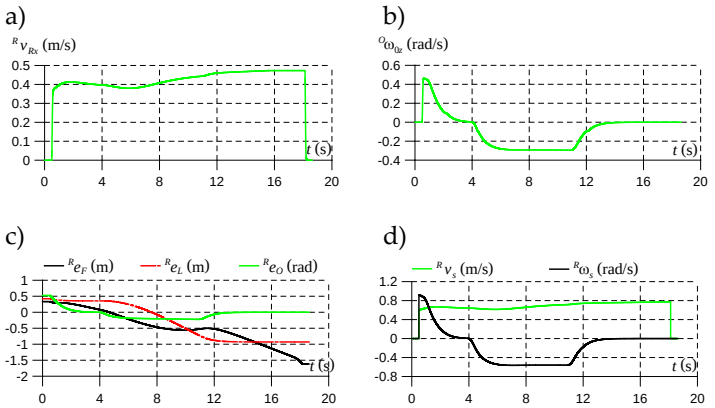

Fig. 11. Time histories of velocities, errors and control signals for the first desired motion trajectory, ${}^{O}\mathbf{q}_{0}$ = [–0.5 m,–0.2 m,–π/6 rad]^{T} and the posture controller solution no. 6

In the last three figures are shown results of simulation studies for the second desired trajectory of motion and for initial posture ${}^{O}\mathbf{q}_0 = [-0.5\text{ m}, -0.1\text{ m}, \pi/3\text{ rad}]^T$. In Fig. 12 results for solution no. 6 of the posture controller are presented. This time during robot motion linear velocity after reaching maximum value gradually decreases (Fig. 12a). The course error ${}^{R}e_O$ is reduced to zero, whereas the ${}^{R}e_F$ and ${}^{R}e_L$ errors are reduced but not completely eliminated. The control signals ${}^{R}v_s$ and ${}^{R}\omega_s$ do not exceed the assumed boundary values.

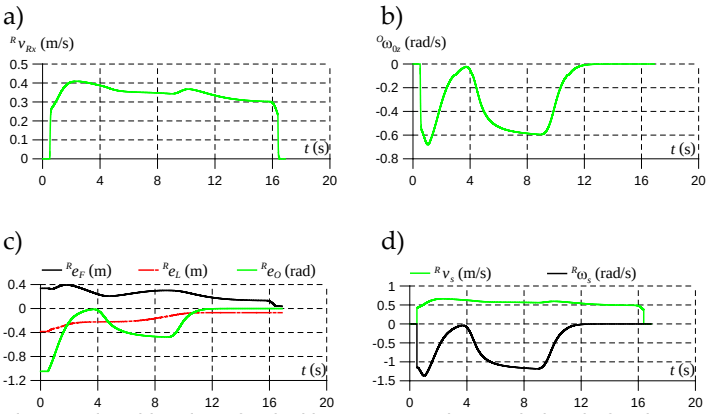

Fig. 12. Time histories of velocities, errors and control signals for the second desired motion trajectory, ${}^{O}\mathbf{q}_0 = [-0.5\text{ m}, -0.1\text{ m}, \pi/3\text{ rad}]^T$ and the posture controller solution no. 6

In the case of posture controller solution no. 5, quite good results are also obtained. As previously the robot linear velocity after reaching maximum value gradually decreases (Fig. 13a). It can be also noticed that the posture errors time histories are similar to those obtained for solution no. 6 (Fig. 13c).

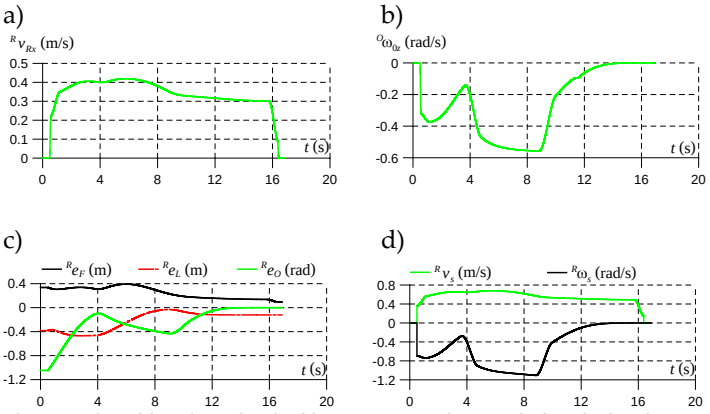

Fig. 13. Time histories of velocities, errors and control signals for the second desired motion trajectory, ${}^{O}\mathbf{q}_0 = [-0.5\text{ m}, -0.1\text{ m}, \pi/3\text{ rad}]^T$ and the posture controller solution no. 5

This time, the worst results were obtained for the solution no. 4 (Fig. 14). This controller eliminates the course error ${}^{R}e_O$ (Fig. 14c) relatively good, but deals much worse with the other types of errors.

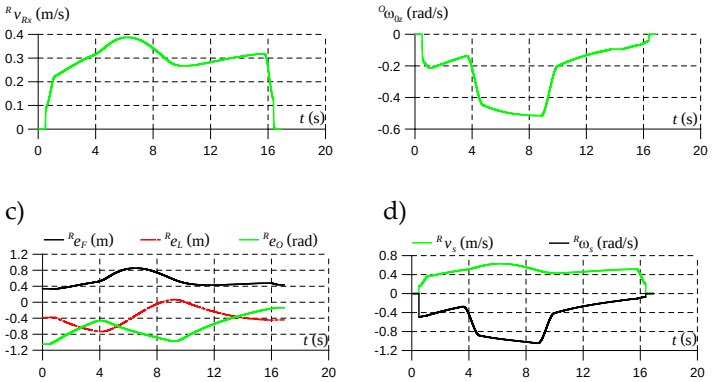

Fig. 14. Time histories of velocities, errors and control signals for the second desired motion trajectory, ${}^{O}\mathbf{q}_0 = [-0.5\text{ m}, -0.1\text{ m}, \pi/3\text{ rad}]^T$ and the posture controller solution no. 4

6 Summary and Future Works

In the work, results of comparative analysis of various solutions of posture controller for tracking control of a four-wheeled skid-steered mobile robot in case of non-zero initial posture (and as consequence non-zero initial posture error) were presented. The research was conducted for two variants of desired trajectory of motion and for three various initial postures.

After comparing the results for the considered solutions of the posture controller in the case of zero initial posture, discussed in the work [19], and for the case of non-zero initial posture which was analyzed in the present work, the largest differences are noticed for the solution no. 6. In this particular case, the performance is the best for zero initial posture, but the worst for the non-zero one.

Because for non-zero initial posture, the best results were obtained for the solution no. 5, and for zero initial posture this solution was the second best ([19]), this solution appears to be the best so far.

In case of the controllers which perform very well for zero initial posture and very poorly for certain non-zero initial conditions, that is, in case of non-zero initial posture errors (e.g. solution no. 6), a different approach should be followed that would additionally involve planning the auxiliary trajectory of motion from the initial robot posture to the correct posture on the main desired motion trajectory.

It should be underlined that the obtained results of robot tracking control with the analyzed solutions of posture controller depend on the introduced modifications and the adopted values of parameters. Therefore the presented conclusions are probably not definitive. Further investigations involving more advanced tuning of controllers, possibly using some alternative approach, are necessary and may lead to different quantitative results of comparative analysis of the controller solutions than presented in this work.

Directions of future works will also include development of new solutions of the posture controller as well as empirical investigations of posture controller solutions with the real ro-

bot aimed at conducting analogous comparative analysis, including the same solutions of the posture controllers as in the present work.

It is also well worth to analyze the following cases:

- the robot in the initial time instant has positive value of the ${}^{O}x_{R0}$ coordinate, that is the ${}^{R}e_{F}$ error is negative, and as a result controller operation strategies can be different: robot either moves backwards, turns 180° and moves forwards or waits until the desired coordinate ${}^{O}x_{Rd}$ is greater than ${}^{O}x_{R0}$;
- the robot in the initial time instant has non-zero posture and auxiliary motion trajectory is generated which guides robot to the main desired motion trajectory;
- the desired motion trajectory includes changes of robot course without changing position (e.g., the robot moves along a straight line, stops and pivot turns towards desired direction).

ACKNOWLEDGMENT

The work has been realized as a part of the project entitled "Dynamics modeling of four-wheeled mobile robot and tracking control of its motion with limitation of wheels slip". The project is financed from the means of National Science Centre of Poland granted on the basis of decision number DEC-2011/03/B/ST7/02532.

REFERENCES

[1] Bayar G., Konukseven E.I., Koku A.B., Mobile Robot Heading Adjustment Using Radial Basis Function Neural Networks Controller and Reinforcement Learning, Proceedings of the 4th WSEAS/IASME International Conference on Dynamical Systems and Controls, 169–174 (2008).

[2] Cao M., Algorithms research of autonomous navigation and control of planetary exploration rover, 2010 Chinese Control and Decision Conference, IEEE, 4359–4364 (2010).

[3] Jaroszek P., Trojnacki M., Localization of the wheeled mobile robot based on multi-sensor data fusion, Journal of Automation, Mobile Robotics & Intelligent Systems, Vol. 9, No. 3, 73-84 (2015).

[4] Jiang Z.-P., Lefeber E., Nijmeijer H., Saturated stabilization and tracking of a nonholonomic mobile robot, Systems & Control Letters 42.5, 327-332 (2001).

[5] Jiang Z.P., Nijmeijer H., Tracking control of mobile robots: A case study in backstepping, Automatica, Vol. 33, 1393–1399 (1997).

[6] Kanayama Y., Kimura Y., Miyazaki F., Noguchi T., A stable tracking control method for an autonomous mobile robot, IEEE International Conference on Robotics and Automation, Cincinnati, OH, USA, 384-389 (1990).

[7] Lakehal B., Amirat Y., Pontnau J., Fuzzy steering control of a mobile robot, International IEEE/IAS Conference on Industrial Automation and Control: Emerging Technologies, Proceedings, 383–386 (1995).

[8] Lauria M. at al., Elastic locomotion of a four steered mobile robot, IEEE/RSJ International Conference on Intelligent Robots and Systems, IROS 2008, 2721–2722 (2008).

[9] Lee J.H., Lin C., Lim H., Lee J.M., Sliding mode control for trajectory tracking of mobile robot in the RFID sensor space, International Journal of Control, Automation and Systems, Vol. 7, No. 3, 429–435 (2009).

[10] Pacejka H.B.: Tire and Vehicle Dynamics, 2nd Edition, SAE International and Elsevier (2005).

[11] Pei X.-Z., Liu Z.-Y., Pei R., Robust trajectory tracking controller design for mobile robots with bounded input, Zidonghua Xuebao/Acta Automatica Sinica, Vol. 29, No. 6, 876–882 (2003).

[12] Perski A., et al., GNSS receivers in engineering practice. Introduction to Global Navigation Satellite Systems, Pomiary, Automatyka, Robotyka, Vol. 17, No. 3, 103–111 (in Polish: "Odbiorniki GNSS w praktyce inżynierskiej. Wprowadzenie do systemów GNSS") (2013).

[13] Ping L.Y., Slip Modelling, Estimation and Control of Omnidirectional Wheeled Mobile Robots with Powered Caster Wheels, Doctorial Thesis, National University of Singapore, Singapore (2009).

[14] Sun D., Dong H.N., Tso S.K., Tracking stabilization of differential mobile robots using adaptive synchronized control, Proceedings of IEEE International Conference on Robotics and Automation, Vol. 3, 2638-2643 (2002).

[15] Toibero J.M., Roberti F., Carelli R., Fiorini P., Switching control approach for stable navigation of mobile robots in unknown environments, Robotics and Computer-Integrated Manufacturing, Vol. 27, No. 3, 558–568 (2011).

[16] Trojnacki M.: Dynamics Model of a Four-Wheeled Mobile Robot for Control Applications – a Three-Case Study, IEEE Intelligent Systems IS'14, Series: Advances in Intelligent Systems and Computing, Springer International Publishing, 99-116 (2014).

[17] Trojnacki M., Dąbek P.: Determination of Motion Parameters with Inertial Measurement Units. Part 2: Algorithm Verification with a Four-Wheeled Mobile Robot and Low-Cost MEMS Sensors, Mechatronics: Ideas for Industrial Applications, Series: Advances in Intelligent Systems and Computing, Springer International Publishing, 253-267 (2015).

[18] Trojnacki M., Dąbek P., Kacprzyk J., Hendzel Z., Comparative Analysis of Posture Controllers for Tracking Control of a Four-Wheeled Skid-Steered Mobile Robot – Part 1. Theoretical Considerations, Advanced Mechatronics Solutions, Series: Advances in Intelligent Systems and Computing, Eds.: Jabłoński R., Brezina T., Springer International Publishing, 583-604 (2016).

[19] Trojnacki M., Dąbek P., Kacprzyk J., Hendzel Z., Comparative Analysis of Posture Controllers for Tracking Control of a Four-Wheeled Skid-Steered Mobile Robot – Part 2. Dynamics Model of the Robot and Simulation Research of Posture Controllers, Advanced Mechatronics Solutions, Series: Advances in Intelligent Systems and Computing, Eds.: Jabłoński R., Brezina T., Springer International Publishing, 605-620 (2016).

[20] Wang K., Liu Y., Li L., Visual servoing trajectory tracking of nonholonomic mobile robots without direct position measurement, IEEE Transactions on Robotics, Vol. 30, No. 4, 1026–1035 (2014).

[21] Wong J.Y.: Theory of Ground Vehicles, 3rd Edition, Wiley-Interscience (2001).

[22] Mobile robots for counter-terrorism (PIAP), http://www. antiterrorism.eu.